PHYSICAL REVIEW E VOLUME 61, NUMBER 4 APRIL 2000

Grains and gas flow: Molecular dynamics with hydrodynamic interactions

Sean McNamara,[1] Eirik G. Flekkøy,[2] and Knut Jørgen Måløy[2]
[1]*The Levich Institute, City College of New York, New York, New York 10031*
[2]*Department of Physics, University of Oslo, P.O. Box 1048 Blindern, 0316 Oslo 3, Norway*

(Received 30 August 1999)

We introduce a simple model for granular flows with hydrodynamic interactions. The hydrodynamic part of the model relies on a coarse grained picture of the granular medium, and is described in terms of the pressure by a local Darcy law. The model thus avoids the large computational cost of solving for detailed hydrodynamic flow fields between grains. The solid phase is described explicitly in terms of grains by event driven molecular dynamics. In the first two test cases, the model is employed to simulate a sedimenting and a fluidized particle bed. It is shown that the qualitative aspects of both phenomena are correctly captured: The sedimenting particles form a sharp upper front and move according to the theoretical prediction, which is also given. When external pressure gradients are applied the bed fluidizes, and spontaneously produces bubbles of the shape observed experimentally. Moreover, these bubbles are seen to merge, as is experimentally observed.

PACS number(s): 81.05.Rm, 47.11.+j, 83.50.−v

I. INTRODUCTION

Particle flow with both direct and fluid interactions between particles is found in a wide variety of systems. These systems include fluidized beds, sedimenting particles, and many granular flows. In fluidized beds [1–3], which are employed industrially in order to enhance mixing processes, a well known instability produces bubbles above a given gas flow rate. In sedimenting systems differences in particle size are known to cause segregation and structure formation [4,5]. In granular flows many distinct phenomena governed by gas−grain interactions are known: even in a stationary settled bed of grains a bubble of air will rise and dissolve as it moves [6]. In gas-filled hourglasses intermittent flow as well as bubble formation will occur due to the volume exchange between the gas and grain phases (see Refs. [7] and [8], which introduce the ‘‘ticking hour glass’’).

Both the fundamental and industrial interest in these phenomena call for reliable numerical modeling. However, their complex nature makes such modeling challenging, and a wide variety of model descriptions with different levels of detail and complexity exist. At the one end particles are described in geometrical detail and the fluid flow is described in full on the subparticle scale, while at the other end both the particle and fluid dynamics are coarse grained at a scale larger than the particles, using conservation relations as the starting point [6,9]. At the detailed extreme the models take the interacting particles to define moving boundary conditions for the Navier-Stokes equations [10–13]. In these models the interparticle fluid flow field represents the finest level of resolution. An intermediate approach is taken by Andrews and O’Rourke [14]. They implemented a method based on the coupling of a continuum description of the gas and a kinetic description (given by a Boltzmann equation) of the particles.

At the detailed end where the description resolves the flow field between the particles, the computational effort required per particle is too large for many applications. However, for many of the large scale phenomena of interest this level of detail in the description is not needed. In the present model the particles constitute the finest level of detail, and are described by molecular dynamics (MD), and the hydrodynamics is described only on a coarse grained level. In the fluid component of the simulation model the particles are considered collectively as a deformable porous medium with a (Carman-Kozeny) permeability given by the local particle density. The main advantage of this scheme is to keep a microscopic description of the particles with the ability this gives to describe strong density variations like shock fronts as well as friction and stagnant particle regions, while avoiding the large computational cost of obtaining the interparticle fluid flow field.

The model of Tanaka and co-workers [15,16] is perhaps the one that most closely resembles the present model. However, the description they gave of the fluid dynamics includes both inertial and drag forces, and is thus given in terms of both the fluid pressure and the velocity field. By neglecting the fluid inertia entirely we are able to describe the interparticle fluid in terms of the pressure alone. The fact that fluid inertia is neglected and the fluid described in terms of the pressure alone gives a model which appears simpler, and presumably more efficient, than existing models with explicit particle descriptions. The conceptual and computational simplicity along with the ability to reproduce physical effects like the bubbling of fluidized beds represent the main virtues of the present approach. Also, while the model by Tanaka *et al.* describes the fluid as incompressible, the present model has a tunable fluid compressibility.

The purpose of the present paper is to study and validate the model. The final application we have in mind concerns locally dense granular flows with hydrodynamic interactions, like the ticking hourglass and related experiments. However, the model is directly applicable to sedimentation processes and fluidized beds [17], and these phenomena provide a natural testing ground. Considered as a model, the main advantage of these phenomena is their ability to resolve individual particle motion and deal with large density contrasts without loss of numerical stability or accuracy, while maintaining computational performance by virtue of a simple description of the fluid. In simulations the sedimenting particles

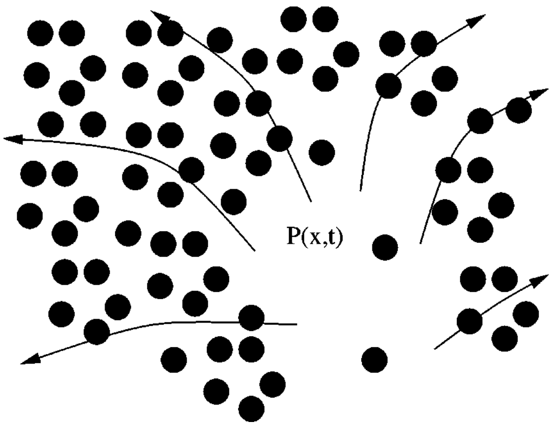

FIG. 1. A conceptual picture of the dynamics. The MD particles move according to Newton's laws while the pressure evolves according to a local Darcy law for which the particles form a porous medium.

form a well known shock front at the upper surface, and below that a roughly constant density [4]. The sedimentation velocity is shown to conform to a theoretical prediction, which follows rather directly from the design of the model. The simulated fluidized bed produces bubbles spontaneously. These bubbles are sharply defined as void spaces, and have a characteristic experimental shape. Also, they exhibit the experimentally observed interaction that make them merge into larger bubbles as they rise [2,18].

II. MODEL

Figure 1 illustrates conceptually the basis for the model. The gas flow, shown by the arrows, takes place between grains that define a local permeability $\kappa(\rho_s)$.

A. Gas dynamics

Although the equation of motion is derived in Ref. [8], we rederive it briefly here for completeness. We shall take the permeability to depend on the local volume fraction $\rho_s = 1 - \phi$ (ϕ is the porosity) of the solid phase according to the Carman-Kozeny relation [19]

$$\kappa(\rho_s) = \frac{a^2}{9K} \frac{(1-\rho_s)^3}{\rho_s^2}, \tag{1}$$

where a is the (spherical) particle radius, and the constant $K \simeq 5$ is obtained experimentally for a packing of spheres.

The evolution equation for the gas pressure is based on the conservation laws for the gas and grain masses. The conservation of the granular volume fraction ρ_s may be written

$$\frac{\partial \rho_s}{\partial t} + \nabla \cdot (\rho_s \mathbf{u}) = 0, \tag{2}$$

where $\mathbf{u}$ is the granular velocity. The conservation of the mass density of the air, ρ_a, may be written

$$\frac{\partial \rho_a}{\partial t} + \nabla \cdot \left(\rho_a \left[\mathbf{u} - \frac{\kappa(\rho_s)}{\mu} \nabla P \right] \right) = 0, \tag{3}$$

where P and μ is the gas pressure and viscosity, respectively. Here the gas current has both an advective term caused by the motion of the grains, and a diffusive term describing the Darcy flow in the local rest frame of reference for the sand. Substituting $\rho_s = 1 - \phi$ into Eq. (2), we obtain

$$-\frac{\partial \phi}{\partial t} + \nabla \cdot [(1-\phi)\mathbf{u}] = 0. \tag{4}$$

Using the isothermal equation of state for an ideal gas, $\rho_a \propto \phi P$, we can write Eq. (3) in the form

$$\frac{\partial(\phi P)}{\partial t} + \nabla \cdot \left(\phi P \left[\mathbf{u} - \frac{\kappa}{\mu} \nabla P \right] \right) = 0. \tag{5}$$

By eliminating $\partial\phi/\partial t$ between Eqs. (5) and (4), a small manipulation gives

$$\phi \left(\frac{\partial P}{\partial t} + \mathbf{u} \cdot \nabla P \right) = \nabla \cdot \left(\phi P \frac{\kappa}{\mu} \nabla P \right) - P \nabla \cdot \mathbf{u}. \tag{6}$$

In this equation the left hand side is just the substantial derivative of the pressure. The first term on the right hand side describes the Darcy flow in the local rest frame of reference of the grains. The last term describes pressure changes due to changes in the grain density. See Ref. [3] for a more elaborate discussion of continuum equations like Eq. (6).

Finally, the numerical solution of Eq. (6) can be simplified by dividing the pressure into average and fluctuating parts: $P = P_0 + P'$. In the experiments we wish to study, the changes in pressure are only a small fraction of atmospheric pressure, so $P' \ll P_0$. Neglecting terms of order $O(P'/P_0)$ in Eq. (6) leads to

$$\phi \frac{\partial P'}{\partial t} = P_0 \nabla \cdot \left(\phi \frac{\kappa}{\mu} \nabla P' \right) - P_0 \nabla \cdot \mathbf{u}. \tag{7}$$

The simplifications leading to this equation are by no means crucial. In applications where they are needed the neglected terms may well be reinserted.

For the numerical implementation it is convenient to nondimensionalize Eq. (7). Writing the characteristic magnitude of the permeability $\kappa_0 = a^2/45$, we may introduce the characteristic grain velocity $U_0 = (\kappa_0/\mu)\rho_g g$, where ρ_g is the mass density of the material that makes up the grains. Introducing the characteristic length scale l, a characteristic time scale $\tau \equiv l/U_0$ follows. The dimensional quantities may then be written in terms of nondimensional (primed) quantities as $P = P_0 P'$, $\mathbf{u} = U_0 \mathbf{u}'$, $x = lx'$, and $t = \tau t'$. Substituting these relations into Eq. (7), we obtain

$$\phi \frac{\partial P'}{\partial t'} = \mathrm{Pe}^{-1} \nabla' \cdot \left(\frac{\phi^4}{(1-\phi)^2} \nabla' P' \right) - \nabla' \cdot \mathbf{u}', \tag{8}$$

where the Peclet number is defined as

$$\mathrm{Pe} = \frac{U_0 l \mu}{P_0 \kappa_0} = \frac{\rho_g l g}{P_0}. \tag{9}$$

The Peclet number derives its name from the fact that it may be interpreted as the ratio between a diffusive time scale and an advective (l/U_0) time scale. Note that it reduces to the ratio between the hydrostatic pressure $\rho_g lg$ caused by the grains and the background pressure P_0. The simplifications leading to Eq. (7) imply a small Peclet number. In the simulations that follow, we use $\mathrm{Pe}=2\times 10^{-4}$.

Equations (6) and (1) describe fluid flow where the fluid inertia may be neglected. This is generally possible when the Reynolds number [20] is small or the problem at hand is such that inertia effects are not important. The Reynolds number is small when the particles are small. With air as the fluid and the particles glass spheres a freely falling particle will acquire a Reynolds number of the order 1 when the particle diameter is around 0.1 mm. This implies that particles must be small. However, when particles become larger the description does not break down in a dramatic way as the first corrections in the Reynolds number amount to small corrections in the pressure forces on the particles. As fluid inertia becomes increasingly important, however, it affects not only the fluid-particle coupling but also the fluid dynamics itself, and in these cases an equation describing the flow of fluid momentum, like the Euler equation [16], is needed.

B. Particle dynamics

The particles evolve according to Newton's second law:

$$m\frac{d\mathbf{v}}{dt}=m\mathbf{g}+\mathbf{F}_I-\frac{\nabla P}{\rho}, \tag{10}$$

where ρ is the number density of particles, $\mathbf{g}$ is the gravity, m is the particle mass, $\mathbf{F}_I$ is the interparticle force, and $\rho=\rho_s\rho_g/m$ is the number density. What distinguishes the present model from conventional models of granular materials is the pressure force per particle $\nabla P/\rho$. It is the pressure gradient obtained from the continuum equation (6), distributed over the particles present in that volume.

Nondimensionalizing Eq. (10) gives

$$\mathrm{Fr}\frac{d\mathbf{v}'}{dt'}=-\hat{\mathbf{z}}+\frac{\mathbf{F}_I}{mg}-\mathrm{Pe}^{-1}\frac{\nabla' P'}{\rho_s}, \tag{11}$$

where $\hat{\mathbf{z}}$ is a unit vector pointing upwards, and Fr has the form of a Froude number

$$\mathrm{Fr}\equiv\frac{U_0^2}{gl}=\frac{U_0/g}{\tau}. \tag{12}$$

The Froude number can be considered as the ratio between two time scales: U_0/g, the time it takes for a falling particle to accelerate from rest to U_0; and $\tau=l/U_0$, the time for a particle falling at speed U_0 to travel a distance l.

In this paper, we use a version of the ''time-of-contact model'' [21], which is an event-driven algorithm to solve Eq. (10). Soft sphere molecular dynamics [22] and contact dynamics [23] could be used instead. In the event-driven method, the output velocities after a collision are computed directly in terms of the input velocities. If $\mathbf{v}$ is the relative velocity between two particles, and $\hat{\mathbf{n}}$ is a normal vector pointing along the line of centers, the normal component of the output velocity $\mathbf{v}'$ is $\mathbf{v}'\cdot\hat{\mathbf{n}}=-r\mathbf{v}\cdot\hat{\mathbf{n}}$, where $r\leqslant 1$ is the restitution coefficient. When $r<1$ the collisions are dissipative, and setting $r=1$ conserves energy. The velocities perpendicular to $\hat{\mathbf{n}}$ are left unchanged: the particles are perfectly smooth, so we can ignore their rotation. Collisions between a particle and the walls can be considered in the same way, except that the wall has infinite mass.

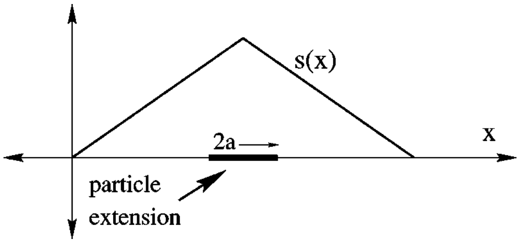

FIG. 2. The particle halo function.

The algorithm for computing the grain trajectories is outlined below.

(1) Advance all particles by the time step Δt, assuming the particles do not interact. Since Δt must be chosen so that particles move only a small fraction of their diameter each time step, the pressure force can be taken as a constant during the short time Δt. Therefore, the particles are advanced along parabolic line segments, corresponding to free flight in a constant force field.

(2) Compile a list of all overlapping particles.

(3) Scan through the list of overlapping particles. If any pair has relative velocities such that the two particles are approaching each other, implement a collision between these two particles. There are two types of collisions: energy conserving and dissipative. If a particle has already suffered a collision in the current or preceding time step, then all collisions involving that particle are energy conserving. Otherwise, they are dissipative. This rule is necessary to avoid inelastic collapse (an infinite number of collisions in finite time [22]). Repeat this step until all pairs of particles are separating. Then go to step (1).

We now need to define ρ and $\mathbf{u}$ in terms of the particle positions and velocities $\mathbf{v}_i$ (i labels individual particles). In order to obtain a continuous density field we will distribute the particle mass in a halo which goes continuously to zero around the particle. This is a standard procedure, and is done by introducing the halo function

$$s(\mathbf{x}-\mathbf{x}_0)=\begin{cases}\left(1-\frac{|x-x_0|}{l}\right)\left(1-\frac{|y-y_0|}{l}\right), & |x-x_0|,|y-y_0|<l\\ 0 \quad \text{otherwise}, & \end{cases} \tag{13}$$

where $\mathbf{x}$ is the particle position and $\mathbf{x}_0$ is the position of a site in the lattice on which P is computed. This function is shown in Fig. 2. The lattice constant is l, and s has the property that it distributes a particle mass over the four nearest lattice sites, i.e., over a region larger than the particle interaction radius. This follows from the observation that

$$\sum_k s(\mathbf{x}-\mathbf{x}_k)=1, \tag{14}$$

where k labels the nearest lattice sites ($k=1,\ldots,4$ on a two-dimensional square lattice). The on-site mass density and velocity $\mathbf{u}$ are now easily defined as

$$\rho(\mathbf{x}_0)\equiv\sum_{i=1}^{N} s(\mathbf{x}_i-\mathbf{x}_0), \tag{15}$$

$$\mathbf{j}\equiv\rho\mathbf{u}(\mathbf{x}_0)\equiv\sum_{i=1}^{N} s(\mathbf{x}_i-\mathbf{x}_0)\mathbf{v}_i\,, \tag{16}$$

where N is the particle number and $\mathbf{v}_i$ the particle velocity. The advantage of these definitions is that ρ and $\mathbf{u}$ now vary smoothly as functions particle positions. The divergence $\nabla\cdot\mathbf{u}$ is evaluated as a finite difference.

Just as the halo function may be used to obtain smooth particle input to Eq. (6), it may be used the other way; to distribute the pressure forces on the particles. The pressure gradient term in Eq. (10) is evaluated at point $\mathbf{x}$ as

$$\frac{\nabla P}{\rho}=\sum_k s(\mathbf{x}-\mathbf{x}_k)(\nabla p)_k/\rho_k\,, \tag{17}$$

where the sum is taken over all grid points, $(\nabla p)_k$ is the pressure gradient at grid point k, and ρ_k is the density. Since the halo function is nonzero only at the four nearest grid points, there will be only four terms in the sum. Recall that ∇p is the rate at which momentum is being transferred from the fluid to the particles. Equation (17) simply states that a particle's share of the momentum deposited at a certain grid point is proportional to that particle's contribution to the density at that same grid point.

C. Implementation

For the model to work in practice it is necessary to introduce a cutoff $\rho_{\min}$ on the density. This has both physical and numerical reasons. Physically there is no sense in defining a permeability field if the particle density is too low. The Carman-Kozeny permeability gives a reasonable prediction only when $\rho_s>0.25$ [24]. Numerically the pressure computations will encounter problems in the form of instabilities both when the permeability becomes too high and when the source term becomes too erratic, as will happen when $\rho_s\rightarrow 0$. Therefore, we shall take $\rho_s=\rho_{\min}$ wherever the measured density in Eq. (15) is less than $\rho_{\min}$. This introduces a cutoff on the permeability, $\kappa<\kappa(\rho_{\min})$. Likewise, when the pressure force on the dilute particles are computed, we shall use $\rho_{\min}$ in place of the actual density when it is too small. This implies that the pressure ''feels'' a permeability corresponding to a higher than actual particle density. Correspondingly, the particles are subjected to the force $\nabla P/\rho=\nabla P/\rho_{\min}$, when $\rho_s<\rho_{\min}$. This means that the particles in the volume cell ΔV corresponding to a lattice site will not absorb the entire force $\nabla P\Delta V$ when $\rho_s<\rho_{\min}$. However, due to the overestimate made by $\kappa(\rho_s)$ in dilute regions, the force per particle will still be larger than the single particle Stokes drag [20]. This means that the error made by introducing the cutoff is mainly that dilute particles fall somewhat more slowly than they should.

Although the practical implementation of the present model in three dimensions is not significantly harder than in two dimensions, we wish to simulate a two-dimensional (2D) system because it is numerically less expensive. However, the Carman-Kozeny equation (1) is a three-dimensional relation as it gives the permeability in terms of the volume fraction of spheres ρ_s, and we wish in the end to compare our results to real three-dimensional experiments. Consequently we need to transform the area fraction of grains in the simulations $\rho_s^{(2D)}$, to the volume fraction ρ_s in such a way that the closed packed value of $\rho_s^{(2D)}$ corresponds to the closed packed value of ρ_s. This is approximately achieved by the transformation $\rho_s=(2/3)\rho_s^{(2D)}$, which we use in the following.

In the simulations we use a distribution of particle sizes to avoid the two-dimensional hexagonal ordering. To improve the relation between the two- and three-dimensional packing densities the closed packed value of $\rho_s^{(2D)}$ will eventually be measured and compared to the three-dimensional random closed packed values. For the present validation process however, this is not needed, and we use the 2/3 factor.

III. SEDIMENTATION

The simplest application of our model, and one that corresponds to a common experimental measurement, is the determination of sedimentation velocities. A volume is initially filled with a uniform mixture of gas and particles, and then the particles are allowed to settle. Experimentally, one observes a sharp boundary between the clear fluid at the top of the container and the particle phase below. This front moves with a well defined velocity, called the sedimentation velocity, which depends on the initial density of the particles. This experiment is easy to simulate; in Fig. 3, we show a typical snapshot from a simulation: the sharp front at the top of the vessel is visible. Another feature is the variations of particle density which form below the front, not unlike the structure formation observed in Batchelor and van Rensburg's sedimentation experiments with two particle sizes [4]. In Fig. 4, we compare the sedimentation velocities observed in the simulations with theoretical values predicted by assuming that the density below the sedimentation front is uniform, and the particles fall without accelerating.

Since the particle volume that is transported downwards must be compensated for by an equal volume upflow of fluid, it is a simple matter to derive a theoretical value for the sedimentation velocity. The conservation of volume means that

$$(1-\phi)\mathbf{u}=-\mathbf{u}+\frac{\kappa(\phi)}{\mu}\nabla P, \tag{18}$$

where $\mathbf{u}$ is the local velocity of the grains and the other quantities are as defined previously. Solving this equation for $\mathbf{u}$, we obtain

$$\mathbf{u}=\frac{\kappa(\phi)}{\mu(2-\phi)}\nabla P. \tag{19}$$

Now the neglect of inertial effects means that the pressure forces must balance the grain weight, i.e., $\nabla P=\rho_s\rho_g\mathbf{g}=\rho_g(1-\phi)\mathbf{g}$, where $\rho_s\rho_g$ is the bulk density of the grains,

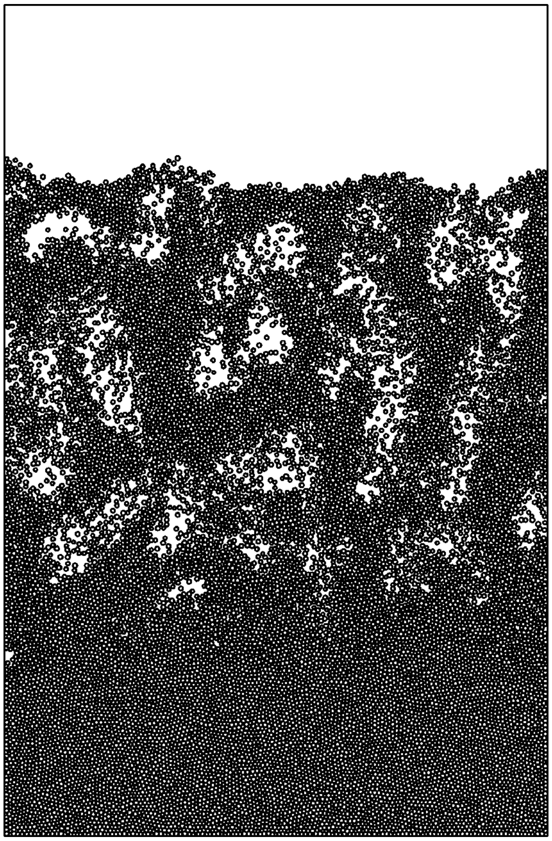

FIG. 3. Simulation of a sedimentation experiment. There are 18 104 particles, and the size of the domain is $62l \times 92l$. The values of the dimensionless numbers are Pe=0.0002 and Fr=1. This picture shows a snapshot at $t = 30\tau$. The walls are perfectly smooth.

ρ_g is the density of the material that make up the grains, and $\mathbf{g}$ is the acceleration of gravity. Now using Eq. (1), we obtain the sedimentation velocity

$$\mathbf{u} = -U_0 \frac{(1-\rho_s)^3}{\rho_s(1+\rho_s)} \hat{\mathbf{z}}, \tag{20}$$

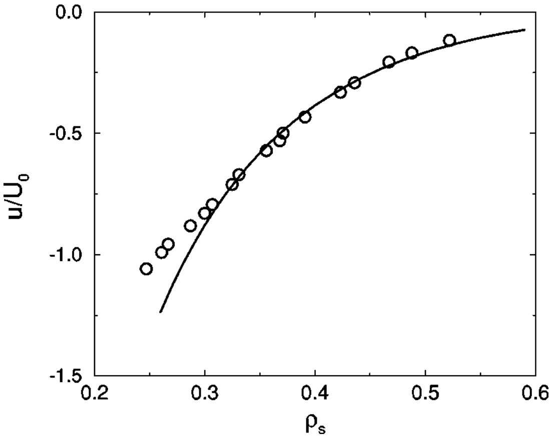

FIG. 4. The sedimentation velocity u, scaled by the typical velocity U_0, as a function of granular volume fraction ρ_s. Each data point corresponds to the results of one simulation at a different initial density. The solid line shows the theoretical result shown in Eq. (20).

where as before $U_0 = a^2 \rho_g g / (45\mu)$.

Figure 3 shows a snapshot of a sedimentation simulation, and Fig. 4 the sedimentation velocity $v_y = u/U_0$ which is measured by averaging over a series of such simulations. Each simulation runs for 50τ, and data are recorded every $\Delta t = 10\tau$. First, average density and velocity profiles are obtained by averaging horizontally. Then, to exclude the settled material at the bottom of the simulation, points with a velocity of less than half the maximum are excluded. To exclude the data points contaminated by the clear region above the settling material, the maximum density of the remaining points is found, and points with less than two-thirds of this density are also excluded. The remaining points are averaged to give a single (ρ, v_y) pair for each time. Then the five points for each simulation are combined to give the single point on the graph. Each simulation has 18 104 particles, and a container width of $60l$, with the height adjusted to give the desired density (it ranges from $60l$ to $124l$). The particles have diameters uniformly distributed in $[0.7d_{\max}$ and $d_{\max}]$, where $d_{\max} = 0.5l$. The coefficient of restitution is $r = 0.8$.

The full line in Fig. 4 shows the theoretical result for homogeneous sedimentation Eq. (20). In spite of the density inhomogeneities shown in Fig. 3, the observed sedimentation values agree well with the theoretical prediction when $\rho_s > 0.3$. We attribute the discrepancy between measurement and theory for $\rho_s < 0.3$ to the presence of regions where the local density ρ falls below $\rho_{\min} = 0.25$. These regions are caused by local density fluctuations, and here the permeability $\kappa(\rho_{\min})$ is smaller than $\kappa(\rho)$. Consequently, the measured settling velocity becomes smaller than the velocity predicted by the theory which does not include the effect of the density cutoff.

IV. FLUIDIZED BEDS

As a next test of the model we inject a constant flux of air at the bottom while removing an equilivalent flux from the top in order to produce the bubbling behavior as observed experimentally in gas fluidized beds [1,17,18]. The air is injected by adjusting the pressure in the bottom row of grid points according to the assumption that the air is isothermal. We specify the amount of air by the volume it would occupy if $P = P_0$. Thus a volume injection of ΔV is implemented by a pressure increase $\Delta P = -P \Delta V / V$, where V is the volume of the region where the pressure is increased. Thus, in Fig. 5, a total of $240l^2$ is injected at the bottom, and the equivalent amount is removed from the top. The formation of bubbles is a salient phenomenon in gas–grain flow, of which the model captures the main features.

Figure 5 shows a time series of a fluidization simulation with initial alternating layers of black and white particles. The particles differ by their color only. The computation was carried out with 18 104 particles and the size of the domain is $60l \times 84l$. A (two-dimensional) volume of air of $240l^2$ was injected uniformly across the bottom during the first 20τ of the simulation. The entire simulation took about 3 h on a workstation.

Three main features of this simulation should be noted. First the bubbles form spontaneously when the pressure difference is turned on. Second, small bubbles coalesce as they move upwards, forming larger bubbles. Finally, the shape of

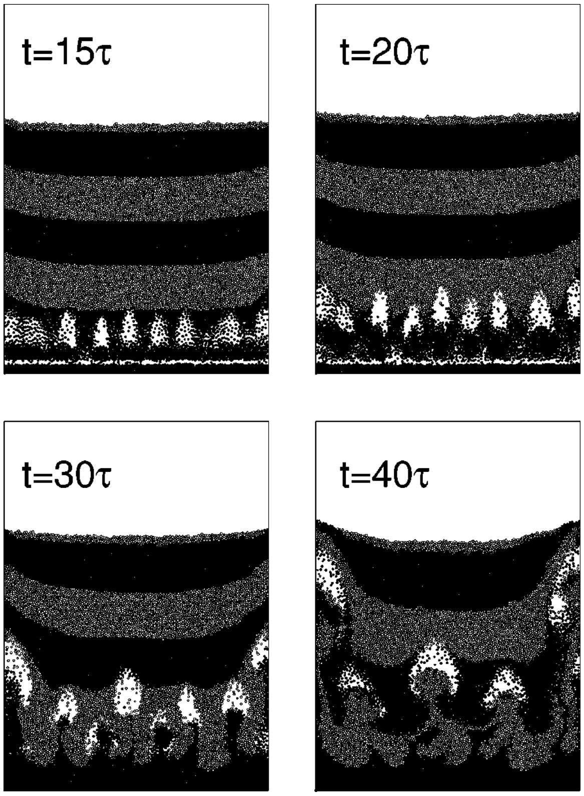

FIG. 5. A time sequence showing the simulation of fluidization. The times are given in dimensionless units. The dimensionless numbers were Pe = 0.0002 and Fr = 1.

the bubbles have the same qualitative features that are observed experimentally [18]. The two first features are also seen experimentally [1,18]. The first and last of the above features were also observed in the simulations of Kawaguchi *et al.* [16]. We note that due to the lack of sliding friction between the particles in the present simulations, the system may start forming bubbles at a denser state than in real systems. Furthermore, the bubbles next to the walls rise abnormally quickly because there is no friction at the walls. The stationary layer of particles at the very bottom is caused by the discretization of the pressure field, and is a numerical rather than physical effect.

V. CONCLUSION

In conclusion we have introduced a model where grain and gas flow couples. This has been done with a guiding principle of maximizing the conceptual and numerical simplicity. For that reason the particles move without rotation and friction, though there is a coefficient of restitution, and fluid that is inertia is neglected. This allows for a very simple description as the fluid is described in terms of a Darcy law, and the particles in terms of event-driven molecular dynamics. In both fluidization phenomena and granular flows there is often a multitude of different scales that need to be resolved. For that reason numerical efficiency is often crucial, and the problem may only be modeled if less relevant information and details of the process are discarded. The result of the simplification made in the present model is a relatively efficient and robust computational scheme with most of the versatility of more involved models. In particular the model shows much promise for the application to granular flows, to which it is now being applied.

The model has been implemented on two test problems—sedimentation and fluidization. The sedimentation velocity measured in the simulations agreed with the anticipated theoretical velocity, save for corrections due to structure formation in the sedimenting bed. In the case of fluidized beds the simulations reproduced the key qualitative features known from experiments, i.e., spontaneous bubble formation, coalescence of these bubbles, and the characteristic bubble shapes.

---

[1] J. F. Davidson, in *Mobile Particulate Systems*, edited by E. Guazzelli and L. Oger (Kluwer, New York, 1995), p. 197.
[2] J. F. Davidson and D. Harrison, *Fluidization* (Academic Press, New York, 1971).
[3] D. Gidaspau, *Multiphase Flow and Fluidization* (Academic Press, San Diego, 1994).
[4] G. K. Batchelor and R. W. Janse van Rensburg, J. Fluid Mech. **166**, 379 (1986).
[5] G. K. Batchelor, J. Fluid Mech. **193**, 75 (1988).
[6] E. G. Flekkøy and K. J. Måløy, Phys. Rev. E **57**, 6962 (1998).
[7] X. L. Wu, K. J. Måløy, A. Hansen, M. Ammi, and D. Bideau, Phys. Rev. Lett. **71**, 1363 (1993).
[8] T. L. Pennec, K. J. Måløy, E. G. Flekkøy, J. C. Messager, and M. Ammi, Phys. Fluids **10**, 3072 (1998).
[9] S. Dasgupta, R. Jackson, and S. Sundaresan, Powder Technol. **96**, 6 (1998).
[10] D. F. M. A. van der Hoef and A. J. C. Ladd, Phys. Rev. Lett. **67**, 3459 (1991).
[11] A. J. C. Ladd, J. Fluid Mech. **271**, 285 (1994).
[12] A. J. C. Ladd, J. Fluid Mech. **271**, 309 (1994).
[13] W. Kalthoff, S. Schwarzer, and H. J. Herrmann, Phys. Rev. E **56**, 2234 (1997).
[14] M. J. Andrews and P. J. O'Rourke, Int. J. Multiphase Flow **22**, 379 (1996).
[15] T. Tanaka, T. Kawaguchi, and Y. Tsuji, Int. J. Mod. Phys. B **7**, 1889 (1993).
[16] T. Kawaguchi, T. Tanaka, and Y. Tsuji, Powder Technol. **96**, 129 (1998).
[17] K. S. Lim, J. X. Zhu, and J. R. Grace, Int. J. Multiphase Flow **21**, 141 (1995).
[18] P. N. Rowe, in *Fluidization* (Academic Press, London, 1971), Chap. 4, p. 121.
[19] P. Carman, Trans. Inst. Chem. Eng. **15**, 150 (1937).
[20] L. D. Landau and E. M. Lifshitz, *Fluid Mechanics* (Pergamon Press, New York, 1959).
[21] S. Luding and S. McNamara, Granular Matter **1**, 111 (1998).
[22] L. Brendel and S. Dippel, in *Physics of Dry Granular Media*, edited by H. J. Herrmann, J.-P. Hovi, and S. Luding (Kluwer, Dordrecht, 1998), p. 313.
[23] F. Radjai and D. Wolf, Granular Matter **1**, 3 (1998).
[24] A. Zick and G. Homsy, J. Fluid Mech. **115**, 13 (1982).